This is a preprint, the final version is subject to change, of the American Mineralogist (MSA)
Cite as Authors (Year) Title. American Mineralogist, in press.
(DOI will not work until issue is live.) DOI: http://dx.doi.org/10.2138/am.2014.4738

Revision 2

A variable-temperature neutron diffraction study of serandite: A Mn-silicate framework with a very strong, two-proton site, hydrogen bond

Edward R. Williams and Mark T. Weller

Department of Chemistry, University of Bath, Claverton Down, Bath, BA2 7AY, UK.

E-mail: m.t.weller@bath.ac.ukcontrol

;

Tel: +44 (0) 1225 386531;

Abstract A variable-temperature powder neutron diffraction study of serandite, $Na(Mn,Ca)_2Si_3O_8(OH)$, has been undertaken over the temperature range 4 – 800 K to investigate the behaviour of the very strong hydrogen bond in this mineral. At 4 K the O(D)…. O(A) distance in serandite has been determined to be extremely short at 2.413(10) Å. The distribution of hydrogen along the O3…..O4 direction at low temperatures confirms that reported previously at room temperature with one site, bonded to O3, strongly, but not exclusively, favoured; the origin of the occupation of this preferred site has been assigned to additional weak hydrogen bonding interactions. At higher temperatures the hydrogen distribution along the O3…O4 direction becomes increasingly random as the thermal energy and motion outweigh the weak hydrogen bonding. The data also show that calcium substitutes only on one manganese site, Mn2 in the mineral structure.

Keywords *Hydrogen bonding, Serandite, Neutron powder diffraction, Variable-temperature*

Introduction

The hydrogen bond is one of the most important interactions in determining the properties of active compounds and the physical properties of materials and minerals (Perrin, 2010). Hydrogen bonding controls polymorphism in numerous pharmaceuticals (Ting et al., 2010), the three-dimensional structures of proteins and saccharides, solvent properties, and the ferroelectric behavior of materials such as potassium dihydrogen phosphate (Grimm et al., 1970). Silicate minerals containing hydrogen bonded OH-groups are of great interest, due to their potential as models for the incorporation of water into feldspars as hydroxyl defects and in developing an understanding of hydrogen incorporation into the high-pressure silicates of the Earth's mantle. The level of water incorporation can play a major role in the properties of the materials, such as mineral strength, melting temperature, reactivity and electrical properties (Bell and Rossman, 1992; Farver and Yund, 1990).

As the neutron scattering length of hydrogen is comparable to many of the other atoms in naturally-occurring silicates, neutron diffraction techniques are ideally suited for study any changes in the hydrogen configuration within strong hydrogen bonds. However, there is only a limited number of examples where such methods have been successfully applied in silicate materials containing strong hydrogen bonds. One such example is the room temperature study into the double-well potential of the hydrogen bond in serandite (Jacobsen et al., 2000), as is the variable temperature NPD study into the structure of the rare aluminosilicate ussingite (Williams and Weller, 2012). In the latter case remarkable behaviors were observed, including negative thermal expansion at temperatures below 50 K and monotonic expansion of the O(donor) - H distance, with perfect asymmetric ordering up to 850 K. The hydrogen bond distances in these minerals, as defined through the O(donor)-O(acceptor) distance are very short, below 2.5 Å and are classified as short, strong hydrogen bonds; these values compare with more typical values for the O(donor)-O(acceptor) distance

in mineral hydrates and hydroxides that are in the range 2.6 to 3.0 Å. In this paper we report structural changes observed for the manganese silicate mineral serandite as a function of temperature through application of the variable-temperature neutron powder diffraction technique. A particular focus was the study of any changes in the O-H...O configuration of the very strong hydrogen bond within this mineral. The often contrasting neutron scattering lengths of electronically similar elements also allows for the resolution of mixed sites within these minerals, such as the substitution of Ca^{2+} into Mn^{2+} sites.

Serandite, $NaMn_2Si_3O_8(OH)$, is a salmon-pink manganese pyroxenoid material found in several localities worldwide (Armbruster et al., 1993; Takeuchi et al., 1976); it is known to form a solid solution with pectolite, $NaCa_2Si_3O_8(OH)$. The structure of serandite was first solved by single-crystal X-ray diffraction (SXD) methods by Takeuchi et al. (1976), and consists of wollastonite-type silicate chains running parallel to the *b*-axis, twisted with a 3-repeat along the chain direction. These chains are linked by pairs of edge-sharing MnO_6 distorted octahedra chains, again aligned parallel to the *b*-axis, with the resulting cavities within the three-dimensional structure formed occupied by Na^+ cations (Na-O 2.6-3.0 Å) (Figure 1). The twisted nature of the silicate chain results in a short O...O distance between O3 and O4, 2.453 Å, with the atoms also notably under bonded (bond valence sums of 1.50 and 1.55 respectively). Combined with an ill-defined residual peak approximately 1.25 Å from both O3 and O4, Takeuchi *et al*. postulated the presence of a strong hydrogen bond. A subsequent SXD study by Takeuchi and Kudoh (1977) on a partially Mn-substituted pectolite crystal showed the electron density within the strong hydrogen bond to be closer to O3, suggesting the hydrogen to be bonded to O3. However, the peak was found to be very broad, with a shoulder closer to O4, defined as a second hydrogen position; from this, they proposed the hydrogen bond to be disordered, alternating between O3-H...O4 and O3...H-O4 configurations along the silicate chains.

A combined single crystal X-ray and TOF neutron diffraction study of serandite at ambient conditions was carried out by (Jacobsen et al., 2000), with the aim of resolving the hydrogen position(s) within the very strong hydrogen bond. Careful examination of the observed scattering density and difference-Fourier maps along the O3...O4 direction showed that the distribution of negative scattering density from the hydrogen atom was centered closer to O3 and asymmetrically elongated towards O4, an observation similar to that of the previous SXD studies (Takeuchi and Kudoh, 1977). A two-proton split-site model was proposed, with the second hydrogen atom positioned closer to O4. The resulting model, with refined hydrogen atom positions and occupancies, yielded lower R-values, suggesting an improvement over the previous one-proton site system. The resulting hydrogen atom occupancies are split in favor of bonding to O3 (84:16), but both sites produced reasonable geometries, with O-H and H...O distances and O-H-O angles being 1.074 and 1.078 Å, 1.407 and 1.413 Å and 164.0 and 168° respectively.

A synchrotron SXD experiment by Arakcheeva et al. (2007) investigated the structural variations of minerals in the serandite-pectolite series at both 100 and 293 K. This study of the manganoan pectolite, $Na(Ca_{1.73}Mn_{0.27})[Si_3O_8(OH)]$, did not investigate the two-proton site model, presumably due to the limitations of X-ray diffraction compared with neutron diffraction in locating hydrogen atoms. It did, however, indicate the strengthening of the hydrogen bond with decreasing temperature, with the hydrogen atom moving to a more symmetric position between O3 and O4.

This article describes the first reported determination of the structure of serandite using neutron powder diffraction at 4 K, using the two-proton site model suggested by Jacobsen et al. (2000). The distribution of manganese and calcium over the two octahedrally-coordinated sites in the structure has been determined. Variable-temperature NPD data were then used to model the behavior of the hydrogen atom in the strong asymmetric hydrogen

bond as a function of temperature between 4 and 800 K, focusing on the changes in the occupancies and positions of the two-proton site model.

Experimental - Neutron diffraction

Neutron powder diffraction patterns were collected on a 1g sample of serandite from Mont Hilaire, Canada (phase purity confirmed by PXRD, energy dispersive X-ray spectroscopic analysis (10 measurements) gave the manganese to calcium ratio as ($Mn_{0.965}Ca_{0.035}$)), on the D2B high resolution diffractometer (λ = 1.594 Å) at the ILL, Grenoble (Hewat and Heathman, 1984). The high resolution of this instrument is ideally suited to the study of these minerals, due to their small triclinic unit cell, while it also delivers a medium-high flux that quickly averages the incoherent scattering arising from hydrogen. This provides a smooth background that can be modelled using polynomial functions. However, it should be noted that where strong peak overlap occurs, particularly at high diffraction angles the exact background position can be difficult to ascertain. In such cases the extracted atomic displacement parameters, U_{iso}s, which depend on modelling the variation of reflection intensity accurately over a large diffraction angle, may be poorly determined. Note also the due to the resolution function of D2B (Hewat and Heathman, 1984) producing large peak half-widths above a diffraction angle around 140° such high angle data were excluded from the refinement due to strong peak overlap.

NPD patterns were collected for three hours at five temperatures: 4, 150, 298, 575 and 800 K. The sample was mounted in a cylindrical vanadium can and placed in a DISPLEX cryofurnace (4, 150K), suspended in the beam (298 K) or placed in a furnace (575, 800 K), before cooling/heating to the initial desired temperature. A thermal equilibration time of 15 minutes was allowed between each temperature change and the start of data collection.

Experimental - Data analysis

The unit cell parameters and atomic coordinates of serandite at each temperature were obtained by Rietveld profile refinements (Rietveld, 1969) using the GSAS suite of programs and the EXPGUI graphical user interface (Larson and Von Dreele, 1994; Toby, 2001). Structural refinement against the 4 K data was undertaken starting with the model reported by Takeuchi et al. (1976) focusing initially on the refinement of the framework. Once this was achieved, the position of the hydrogen atom was investigated, with particular focus on the resolution of the split occupancy between both potential wells within the strong hydrogen bond, as suggested by Jacobsen et al. (2000). During refinement all identical atom types, including the two hydrogen atoms, were constrained to have the same atomic displacement parameter (ADP) value, though these values were refined. No correction for extinction was made to the data as previous studies of similar sized samples with higher hydrogen contents have shown negligible effects Henry, P.F et al. (2009).

In addition, the serandite-pectolite series represents a solid solution with substitution of Mn for Ca, both octahedrally coordinated species, across the series. Serandite is the Mn end-member of the series, however a small level of Ca-substitution was found from chemical analysis of the sample studied. Both octahedral sites were refined as mixed Mn/Ca sites and the Mn:Ca ratio extracted, made possible due to the strong contrast between the coherent neutron scattering lengths of Mn (-3.57 fm) and Ca (4.70 fm).

The most suitable structural model for the 4 K data, as indicated by agreement indices of Rietveld refinement (see below), has a split H site with occupancy ratio H16:H17 = 78(4):22(4). This model also has Mn fully ordered at M1, and M2 has a composition 0.95(1)Mn + 0.05(1)Ca. This final model was refined to convergence, using isotropic ADPs for all atoms. The resulting crystallographic parameters are summarized in Table 1, with the profile fit shown in Figure 2.

The crystallographic parameters refined for the 4 K model were used as the starting model for the refinement of the dataset for the next temperature (150 K), the result of which was in turn used for the 298 K refinement and so on iteratively for each successive temperature. A summary of results of the various Rietveld refinements for all temperatures are given in Table 1 and CIFs have been deposited as supplementary material.

Results and Discussion

Inspection of the diffraction patterns collect at each temperature indicated no change in phase over the temperature range studied.

4K structure

After refinement of all non-hydrogen positions, a difference-Fourier map of the neutron scattering density along the O3...O4 direction was generated (in the structural plane defined by O3 and O4, and viewed normal to the (5 0 -5) lattice plane) and showed a broad negative peak, elongated between the two oxygen atoms (Figure 3). The best fitting model of this area of neutron scattering density, as determined from the resulting profile fit factors, R_p, wR_p and χ^2, was a two-proton site model with isotropic ADPs, positioned at the sites shown in Figure 3, and split in favor of H16 (~75:~25), note that within this model refinement of individual anisotropic ADPs for the hydrogen atoms was unstable. This two-site model determined is an improvement giving lower residuals (*Rp*=0.0227, *wRp*=0.0284 and χ^2=1.76) over attempts using a one-proton site model either at a central site or on a single site near either O3 or O4: Placement of hydrogen on a central symmetric site gave χ^2=1.86 (one-proton site, isotropic ADPs) or 1.78 (one proton site, anisotropic ADPs, this also produced an ellipsoid very strongly elongated along the O3-O4 indicative of a split position model). Placement of hydrogen wholly on the H16 site produced poorer profile fitting statistics, χ^2=1.83.

Atom coordinates, isotropic temperature factors, Table 2, and derived interatomic distances and selected bond angles, Table 3, were obtained from the final structural refinement for the 4K data. The d(O3...O4) distance is 2.413(10) Å, being 0.056 Å shorter than that observed at room temperature by Jacobsen et al. (2000) in their single-crystal neutron diffraction (SND) study. Similarly, the H-O distances were found to be shorter than those of the RT-SND results, with H16-O3 and H17-O4 distances of 1.03(2) and 0.96(5) Å respectively [cf. 1.078(3) and 1.074(11) Å]. The occupancies of the two H-sites show a ratio of 0.78(4):0.22 with preponderance bonded to O3 This ratio differs only slightly from that found by Jacobsen et al. (2000) using SND but has the same preference for an O3-H bond; the origins of this variance may result from a slightly different Ca:Mn ratio in the mineral studied or the treatment of ADPs in Jacobsen's work where a higher U_{eq} for one site compared with the other might favor occupancy of this position. Also, the occupation of the two H-sites may be statistical in nature, representing the relative depth of the two energy minima along the O3...O4 direction. The different scattering lengths of Mn and Ca allow for the resolution, with ease, of the occupancies of mixed sites, with one Mn site (Mn1) found to be entirely Mn-ordered, whilst the second site (Mn2) contained 5% Ca.

Structural response on heating

The variations in lattice parameters for serandite in the 4-800 K range is summarized in Figure 4, normalized through division by the 4 K lattice parameter values. No negative thermal expansion was observed, unlike that found for ussingite (Williams and Weller, 2012). The near linear expansion between room temperature and 800 K has a volumetric thermal expansion coefficient, α_V, of 3.34×10^{-5} K^{-1}. Typical exponential expansion is observed along all three axes, with slightly higher rate of expansion observed for the *a*-axis. This effect is likely to arise from the greater number of M-O-M linkages near-parallel to the *bc*-plane, due to the rotational thermal motion of bridging O-atoms, moving perpendicular to the M-O-

195 M direction, having the effect of relaxing, and therefore shortening, the M-M distance
196 (Lightfoot et al., 2001).

197 Difference-Fourier maps were calculated for each temperature. Each showed the
198 negative scattering peak representing the hydrogen atom to be broad, elongated along the
199 O3...O4 direction, and suggesting the two-proton model is correct for all temperatures up to
200 800 K. Using the previous hydrogen atom positions and occupancies as a starting point,
201 initially the occupancies of both hydrogen atom sites for each temperature were refined,
202 followed by positions for one H-site at a time; the U_{iso} values of the hydrogen atoms were
203 constrained to be equal. Figure 5d shows the changes in the occupancies of the sites within
204 the two-proton site model. At lower temperatures, at and below room temperature, there is a
205 clear preference (~80% to 60%) for the hydrogen atom to bond to O3 while at higher
206 temperatures the distribution between the two sites approaches the statistical 50:50.

207 This behavior and the low temperature preference for bonding to O3 can be explained
208 through examination of hydrogen bonding to more distant framework oxygen atoms. Figure 6
209 shows an expanded view of the environment about the split hydrogen site, with two
210 additional hydrogen bonds observed between both hydrogen positions and the O3 and O5
211 silicate oxygen positions. The next nearest oxygen atoms to H16 and H17 are O3' (an oxygen
212 atom forming the donor atom in the nearest hydrogen bond) and O5, respectively; at 4K the
213 distances from H16 to these oxygen atoms are 2.53 and 2.55 Å respectively while for H17 the
214 corresponding distances are 2.55 and 2.85 Å. This has the effect of preferentially stabilizing
215 the H16 site, compared to H17, thus increasing the likelihood of hydrogen being positioned at
216 this site, resulting in the higher occupancy observed at this site. At 575 and 800 K the
217 occupancies of the H-atom sites are almost equal as the thermal energy overcomes the effect
218 of this weak hydrogen-bonded interaction.

The changes in the O3-H...H-O4 configuration are plotted, as a function of temperature, in Figure 5. There is only a small variation in both the O-H bond distances, remaining in the 1.00-1.10 Å range for O3-H16 and 0.94-1.00 Å range for O4-O17, while there is are small increases in the H...O distances (1.47 → 1.55 Å for H17 and 1.41→1.46 for H16). Combined with the increasing O...O distance, this indicates the hydrogen bonding is weaker at higher temperatures, resulting in the system moving towards a symmetric double potential well that is reflected in the changing occupancies of the two hydrogen positions. This weakening of the hydrogen bond is reflected in the observed rapid increase in the O3….O4 separation above 300 K and the derived thermal expansivity of the O3…O4 distance 6.7×10^{-5} K^{-1} far greater than $\alpha_V/3$ (1.1×10^{-5} K^{-1}). At 800 K the bonding environments are nearly identical within a symmetrical double-well having, presumably, a very shallow potential barrier between them. Somewhat unusually there is only a moderate elongation of the O3-H16 distance in this very strong hydrogen bond (Emsley, 1980). A plausible reason for the only moderate lengthening of O-H bonds for these very strong hydrogen bonds may be the close proximity of Na at only ~2.2 Å away from both H atoms. Any significant lengthening of the O-H bonds would be opposed by a strong repulsive H…Na interaction.

Implications

The hydrogen bond is one of the most important interactions in determining the physical properties of minerals (Perrin, 2010) and silicate minerals containing hydrogen bonded OH-groups are of great interest, due to their potential as models for the incorporation of water into feldspars as hydroxyl defects. In this work we have studied as a function of temperature the hydrogen bond in serandite, $NaMn_{0.96}Ca_{0.04}Si_3O_8(OH)$, one of the few silicate materials containing a very strong hydrogen bond. The hydrogen bond in serandite at 4 K was found to be one of the strongest known between two oxygen atoms with the O(donor) –O (acceptor)

244 separation at just 2.413(9) Å (Emsley, 1980). The hydrogen atom was found to be distributed
245 over two sites as described previously in a room temperature SND, over the 4-800 K
246 temperature range. The changes in the O-H bonding and H...O hydrogen bonding, as well as
247 the occupancies of the two sites of the two-proton model approaching equivalence, indicates
248 the system moves towards a symmetric double-well potential, and small separating potential
249 barrier, with increasing temperature. The origin of the asymmetric distribution of hydrogen at
250 low temperatures was found to be additional weak hydrogen bonding interactions for the
251 preferred site. This information should provide the basis for much improved modeling of very
252 strong hydrogen bonds in minerals.
253

254 **Acknowledgements** This research was supported by the EPSRC (EP/G068038/1). We also
255 thank ILL for the provision of neutron beam time under proposal 5-21-1025.

256 **References**

257 Arakcheeva, A., Pattison, P., Meisser, N., Chapuis, G., Pekov, I., and Thelin, P. (2007) New
258 insight into the pectolite-serandite series: a single crystal diffraction study of
259 $Na(Ca_{1.73}Mn_{0.27})$ HSi_3O_9 at 293 and 100 K. Zeitschrift Fur Kristallographie, 222(12).
260 Armbruster, T., Oberhansli, R., Bermanec, V., and Dixon, R. (1993) Hennomartinite and
261 kornite, 2 new Mn^{3+} rich silicates from the Wessels-mine, Kalahari, South Africa.
262 Schweizerische Mineralogische Und Petrographische Mitteilungen, 73(3), 349-355.
263 Bell, D.R., and Rossman, G.R. (1992) Water in earths mantle - the role of nominally
264 anhydrous minerals. Science, 255(5050), 1391-1397.
265 Emsley, J. (1980) Very strong hydrogen bonding. Chemical Society Reviews, 9(1), 91-124.

Farver, J.R., and Yund, R.A. (1990) The effect of hydrogen, oxygen, and water fugacity on oxygen diffusion in alkali feldspar. Geochimica Et Cosmochimica Acta, 54(11), 2953-2964.

Grimm, H., Stiller, H., and Plesser, T. (1970) Neutron measurements on hydrogen bond potential in paraelectric KDP. Physica Status Solidi, 42(1), 207-&.

Hewat, A.W., and Heathman, S. (1984) D2B, a new high-resolution neutron powder diffractometer. Acta Crystallographica Section A, 40, C364-C364.

Henry, P.F, Weller, M.T. and Wilson. C.C. (2009) Powder neutron diffraction in materials with incoherent scattering: An illustration of Rietveld refinement quality from non-deuterated gypsum. Journal of Applied Crystallography, 42, 1176-1188.

Jacobsen, S.D., Smyth, J.R., Swope, R.J., and Sheldon, R.I. (2000) Two proton positions in the very strong hydrogen bond of serandite, $NaMn_2Si_3O_8(OH)$. American Mineralogist, 85(5-6), 745-752.

Larson, A.C., and Von Dreele, R.B. (1994) "General Structure Analysis System (GSAS)". Los Alamos National Laboratory Report LAUR 86-748.

Lightfoot, P., Woodcock, D.A., Maple, M.J., Villaescusa, L.A., and Wright, P.A. (2001) The widespread occurrence of negative thermal expansion in zeolites. Journal of Materials Chemistry, 11(1), 212-216.

Perrin, C.L. (2010) Are Short, Low-Barrier Hydrogen Bonds Unusually Strong? Accounts of Chemical Research, 43(12), 1550-1557.

Rietveld, H.M. (1969) A profile refinement method for nuclear and magnetic structures. Journal of Applied Crystallography, 2, 65-71.

Takeuchi, Y., and Kudoh, Y. (1977) Hydrogen-bonding and cation ordering in Magnet cove pectolite. Zeitschrift Fur Kristallographie, 146(4-6).

Takeuchi, Y., Kudoh, Y., and Yamanaka, T. (1976) Crystal-chemistry of serandite-pectolite series and related minerals. American Mineralogist, 61(3-4).

Ting, V.P., Schmidtmann, M., Wilson, C.C., and Weller, M.T. (2010) Cisplatin: Polymorphism and Structural Insights into an Important Chemotherapeutic Drug. Angewandte Chemie-International Edition, 49(49), 9408-9411.

Toby, B.H. (2001) EXPGUI, a graphical user interface for GSAS. Journal of Applied Crystallography, 34, 210-213.

Williams, E.R., and Weller, M.T. (2012) A variable-temperature neutron diffraction study of ussingite; a strong asymmetric hydrogen bond in an aluminosilicate framework. Physics and Chemistry of Minerals, 39(6), 471-478.

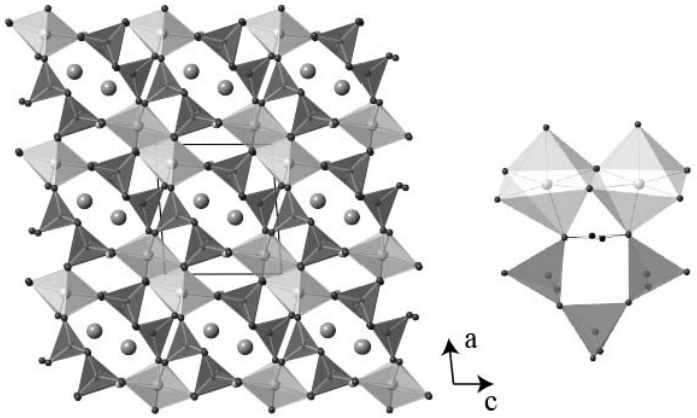

302

303 **Figure 1.** The crystal structure of serandite, viewed down the *b*-axis, with (inset) the position
304 of the strong hydrogen bond. Light and dark grey polyhedra represent those centered on Mn
305 and Si respectively, with O as small grey spheres, large grey spheres represent sodium cations
306 and small black spheres are hydrogen. The hydrogen bond is shown using a dashed line.

307

308

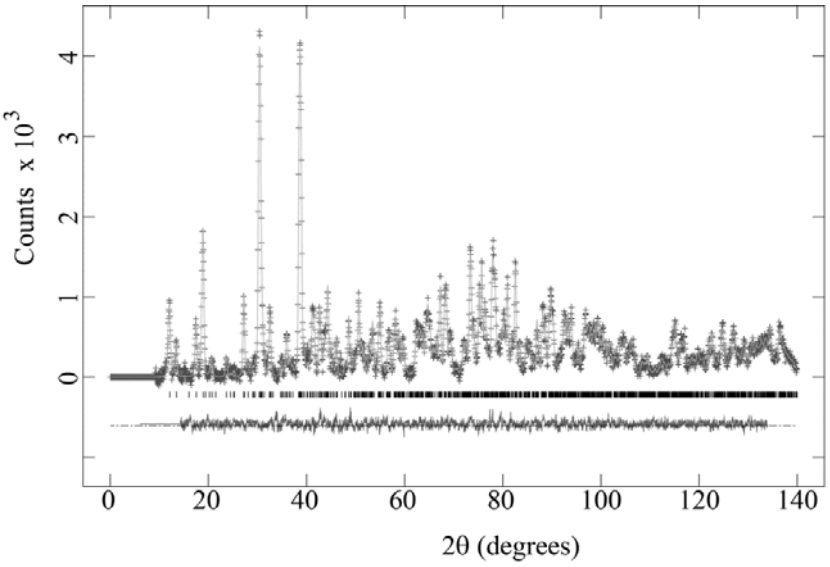

309

310 **Figure 2.** Rietveld profile fit for powder data collected from serandite at 4 K. Crosses
311 represent the observed data, the *upper curve* the calculated profile, the *lower curve* is the
312 difference and the tick marks represent calculated reflection positions

313

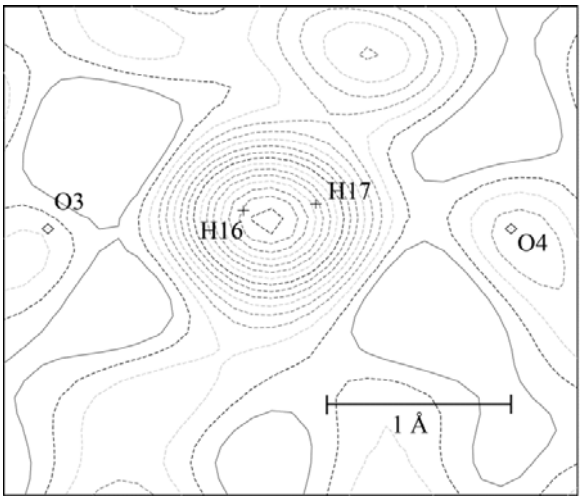

Figure 3. Difference-Fourier map ($F_{obs} - F_{calc}$, with F_{calc} values obtained using just Na, Ca, Mn, Si and O sites) for serandite, viewed normal to the (5 0 -5) lattice plane, showing the two hydrogen atom sites within the elongated negative scattering peak along the hydrogen bond direction. Contour heights are drawn with a 2 fm/Å^3 separation and negative values shown as dashed lines.

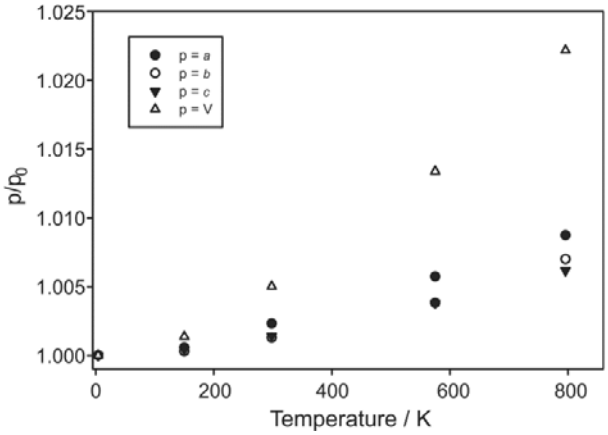

Figure 4. The variation of the lattice parameters of serandite as a function of temperature in the 4-800 K range, with *a*, *b* and *c* normalized by division by p_0 (minimum value for lattice parameter p at 4K). Error bars are within the symbol size

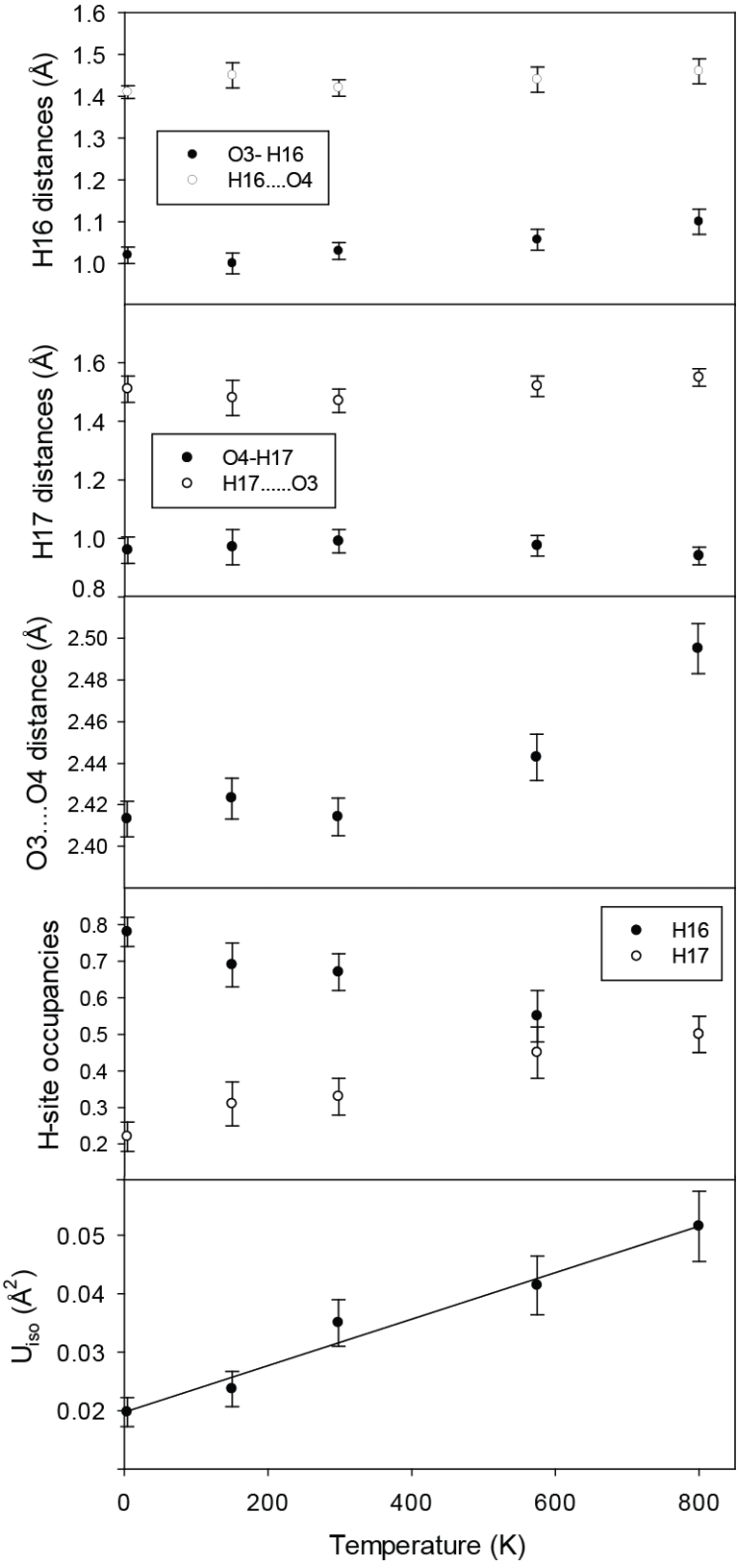

Figure 5. The variation with temperature of the H-site occupancies, O-H, H…O and O…..O distances and U_{iso} (H) values in serandite

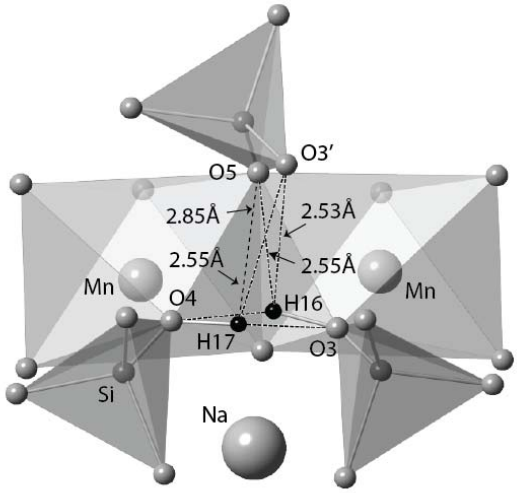

329

330 **Figure 6.** Further, longer range hydrogen bonding stabilizing the two hydrogen atom

331 positions, which influences the occupancies of the split hydrogen atom site

332

333

334

335 **Table 1.** Rietveld refinement results for serandite at 4, 150, 298, 575 and 800 K

Refinement results	4 K	150 K	298 K	575 K	800 K
a	7.6844(4)	7.6888(4)	7.7024(3)	7.7283(5)	7.7513(6)
b	6.8913(4)	6.8934(4)	6.9003(3)	6.9174(5)	6.9384(6)
c	6.7349(4)	6.7378(4)	6.7447(4)	6.7608(5)	6.7761(6)
α	90.438(3)	90.447(3)	90.416(3)	90.362(4)	90.307(5)
β	94.085(3)	94.067(3)	94.044(3)	94.016(4)	94.019(4)
γ	102.777(3)	102.777(3)	102.801(3)	102.822(4)	102.858(5)
V (Å^3)	346.83(4)	347.29(4)	348.60(4)	351.46(5)	354.34(7)
R_p	0.0228	0.0226	0.0226	0.0213	0.0208
wR_p	0.0287	0.0281	0.0282	0.0267	0.0261
R_F^2	0.0364	0.0385	0.0426	0.0409	0.0468
χ^2	1.717	1.667	1.762	1.472	1.339

Space group $P\bar{1}$

336

337 **Table 2.** Atomic coordinates and isotropic temperature factors for serandite at 4 K

Atom site	*x*	*y*	*Z*	U × 10^2 (Å^2)
Mn1	0.8533(16)	0.5896(18)	0.1394(18)	0.25(12)
Mn2[a]	0.8511(21)	0.0863(23)	0.1310(23)	1.05(10)
Na1	0.5598(17)	0.2514(22)	0.3582(18)	1.00(28)
Si1	0.2152(13)	0.4106(16)	0.3457(16)	0.02(13)
Si2	0.2068(14)	0.9442(16)	0.3461(16)	0.02
Si3	0.4536(12)	0.7385(15)	0.1442(13)	0.02
O1	0.6657(9)	0.7956(11)	0.1089(11)	0.45(6)
O2	0.3204(10)	0.7061(12)	0.9395(11)	0.45
O3	0.1784(11)	0.4970(11)	0.5555(12)	0.45
O4	0.1596(10)	0.8419(12)	0.5593(11)	0.45
O5	0.0628(10)	0.3942(11)	0.1667(11)	0.45
O6	0.0531(10)	0.8922(13)	0.1727(11)	0.45
O7	0.4082(11)	0.5344(12)	0.2757(11)	0.45
O8	0.3978(11)	0.9102(12)	0.2871(12)	0.45
O9	0.2582(11)	0.1886(12)	0.3926(10)	0.45
H16[b]	0.1486(25)	0.635(4)	0.5544(33)	1.97(25)
H17[b]	0.141(9)	0.712(16)	0.498(13)	1.97

[*a*] Mn:Ca ratio of 95.0(1.2) : 5.0(1.2)

[*b*] H16:H17 occupancies 0.78(4):0.22(4)

338

339

340 **Table 3.** Selected bond distances and bond angles for serandite at 4 K

Atoms	Distance (Å)	Atoms	Distance/ Angle (Å)	Atoms	Distance/ Angle (Å/°)
Mn1-O1	2.237(14)	Si2-O4	1.633(13)	O3-Si1-O9	105.5(7)
-O2	2.213(15)	-O6	1.580(13)	O5-Si1-O7	110.1(6)
-O3	2.160(14)	-O8	1.612(11)	O5-Si1-O9	111.4(7)
-O5	2.315(14)	-O9	1.665(13)	O7-Si1-O9	101.4(6)
-O5’	2.200(14)	<Si2-O>	1.623	O4-Si2-O6	115.6(8)
-O6	2.298(15)	Si3-O1	1.625(11)	O4-Si2-O8	108.8(7)
<Mn1-O>	2.237	-O2	1.641(11)	O4-Si2-O9	105.6(7)
Mn/Ca2-O1	2.183(17)	-O7	1.653(12)	O6-Si2-O8	114.0(8)
-O2	2.183(18)	-O8	1.665(13)	O6-Si2-O9	110.8(8)
-O4	2.151(17)	<Si3-O>	1.654	O8-Si2-O9	100.8(7)
-O5	2.369(17)	O3...O4	2.413(10)	O1-Si3-O2	114.6(8)
-O6	2.268(19)	O3-H16	1.03(2)	O1-Si3-O7	109.8(7)
-O6’	2.218(17)	O4-H17	0.96(5)	O1-Si3-O8	110.8(7)
<Mn2-O>	2.229	O3...H17	1.63(9)	O2-Si3-O7	109.4(8)
Si1-O3	1.597(12)	O4...H16	1.41(2)	O2-Si3-O8	107.5(8)
-O5	1.605(12)	H16...H17	0.66(6)	O7-Si3-O8	104.3(7)
-O7	1.642(11)			O3-H16-O4	158.6(23)
-O9	1.663(13)	O3-Si1-O5	119.1(8)	O3-H17-O4	160(4)
<Si1-O>	1.627	O3-Si1-O7	107.8(7)		

341

342

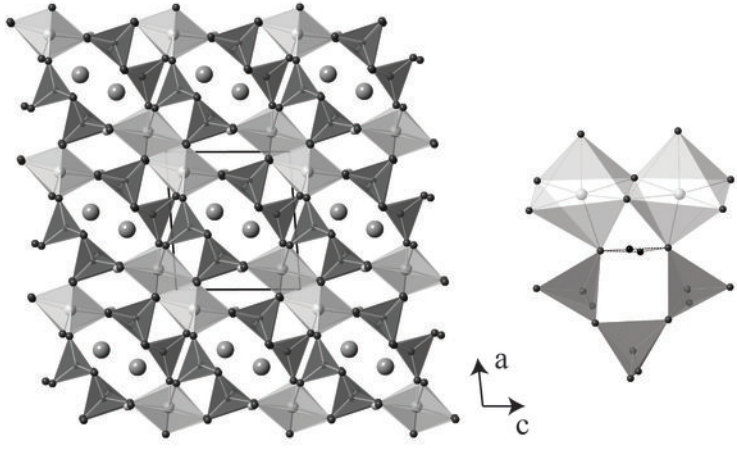
a
c

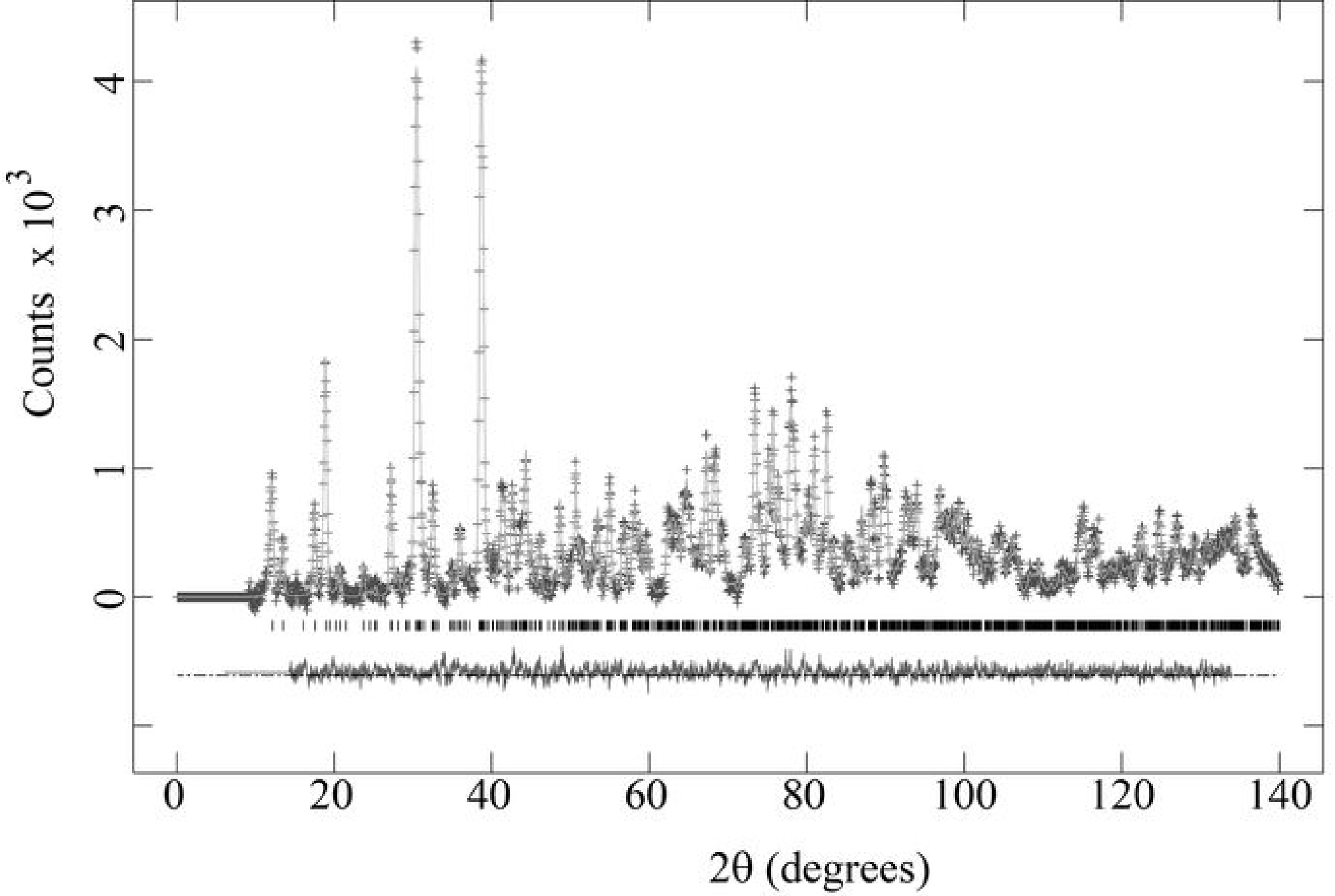
Counts x 10^3
0
1
2
3
4
0
20
40
60
80
100
120
140
2θ (degrees)

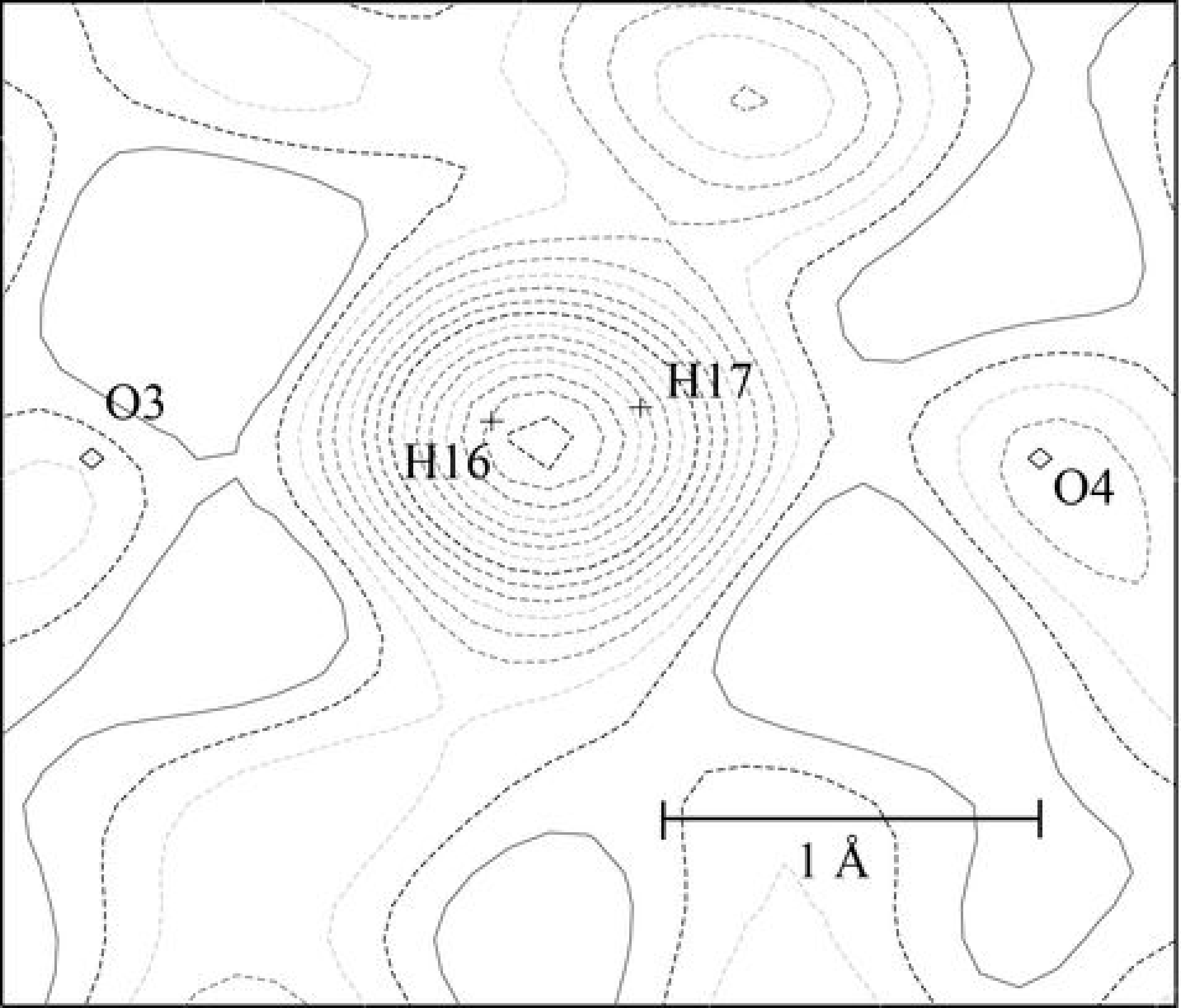
O3
H16
H17
O4
1 Å

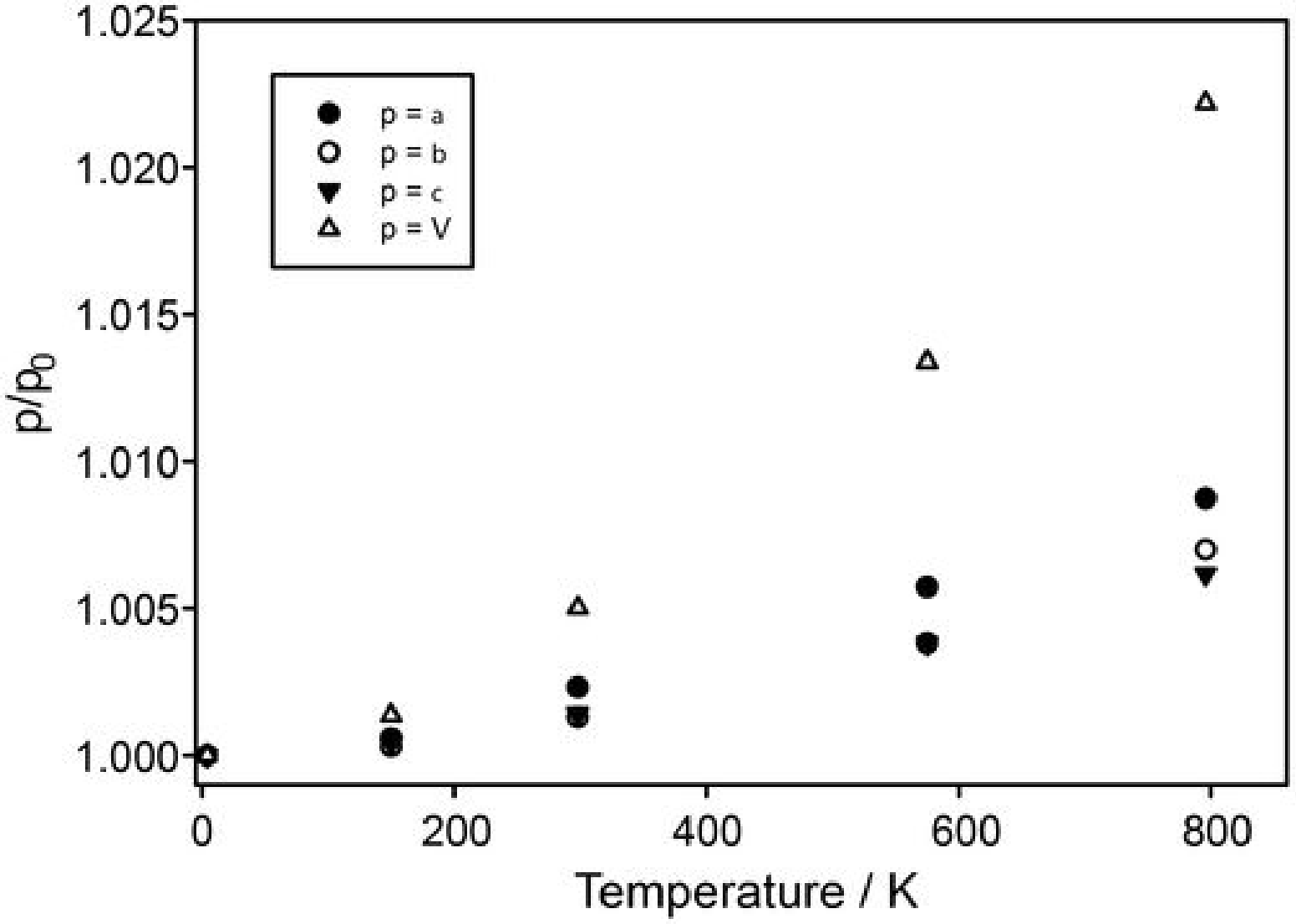
p = a
p = b
p = c
p = V
1.025
1.020
1.015
1.010
1.005
1.000
p/p0
0
200
400
600
800
Temperature / K

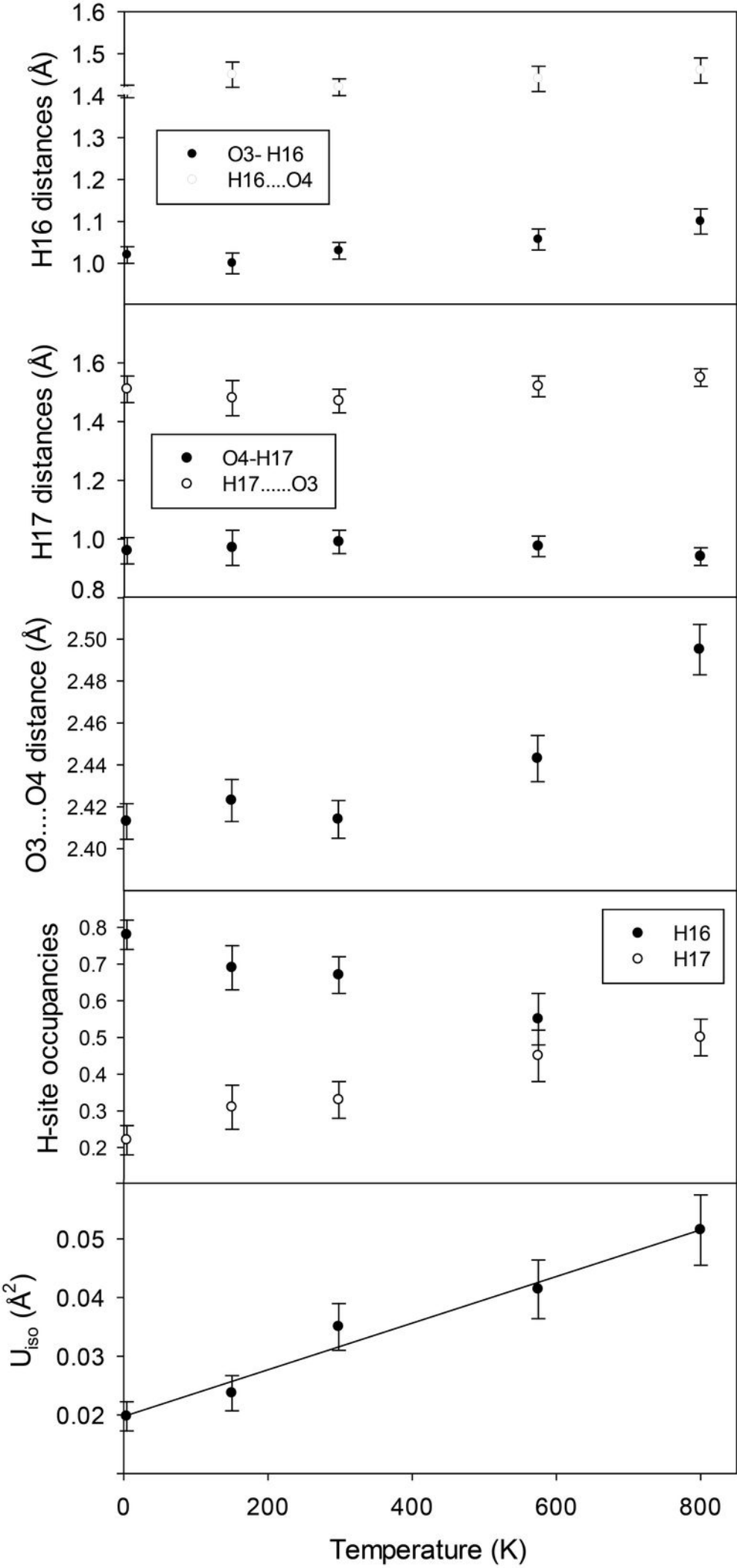
H16 distances (Å)
O3- H16
H16....O4
H17 distances (Å)
O4-H17
H17.....O3
O3....O4 distance (Å)
H-site occupancies
H16
H17
U_{iso} (Å^2)
Temperature (K)

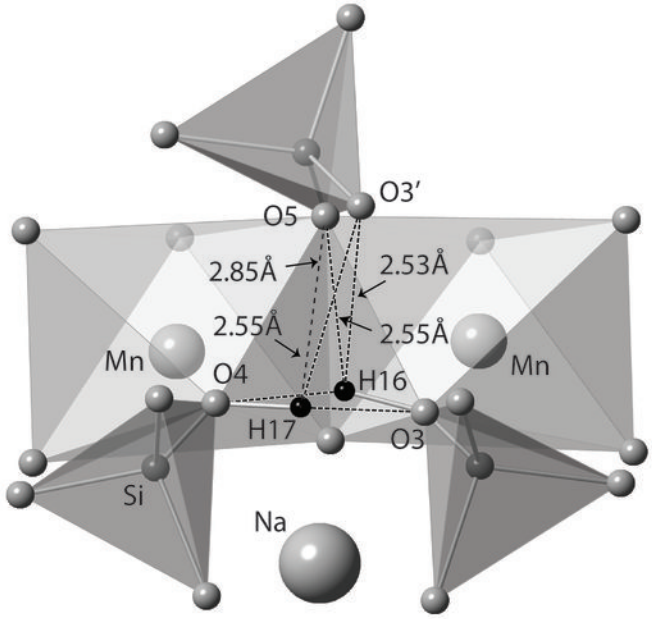
O3′
O5
2.85Å
2.53Å
2.55Å
2.55Å
Mn
O4
H16
Mn
H17
O3
Si
Na